14

Implementation of the Front-End-Module with a Power Amplifier for Wireless LAN

Jong-In Ryu, Dongsu Kim and Jun-Chul Kim
Korea Electronics Technology Institute
South Korea

1. Introduction

Recently, Wireless Local Area Network (W-LAN) market has been continuously growing in many filed and it become mature market. Therefore, a number of companies are researching and developing the W-LAN technology. Normally, W-LAN application is wildly used in the desktop computer, laptop computer, portable device, mobile phone, and so on. These application demands compact, small, low power consumption, slim, and many function in a module. These demands issue that a lot of components are integrated in a module. Low temperature co-fired ceramic (LTCC) continues to be attracted in wireless applications because it can implement a small, compact, and integrated module which embedding passive components by taking advantage of three-dimensional architecture. LTCC has high dielectric constant and low loss tangent that it has some benefits over other material substrates. The size of LTCC is shrunk after process of co-fired which makes some issues in design and implementation of LTCC. In spite of these disadvantages, many researches and companies have been researching and developing many passive components, RF modules, and front-end modules (FEM) by using the LTCC technology.
IEEE 802.11 a/b/g as W-LAN standard has been allocated two frequency bands for 2.4 GHz - 2.5 GHz (IEEE 802.11 b/g) and 5.15 GHz - 5.85 GHz (IEEE 802.11 a). The frequency band of IEEE 802.11 b/g and of IEEE 802.11 a are called as low-band and high-band, respectively.
The implemented W-LAN FEM coves low-band and high-band. It is composed of two matching circuits for low-band and high-band, two Tx low pass filters (LPFs) in order to reject 2nd harmonic frequency of a power amplifier module (PAM), two Rx band pass filters (BPFs) in order to reject interferers as blocker, a Rx diplexer to separate low-band from high-band, a Tx diplexer, a single-pole-double-throw (SPDT) switch for sharing the antenna between the RX and TX paths , and a PAM for low-band and high-band as shown in fig.1. Two Tx LPFs, two matching circuits, Tx diplexer, two Rx BPFs, and Rx diplexer are embedded in LTCC substrate. A DPDT IC and PAM IC are mounted on LTCC substrate. Embedded components are very sensitive to tolerance of LTCC and mutual coupling. A control of process LTCC and a layout of embedded components are important facts and are focused on being considered in design of a FEM. The design and layout are mainly discussed in this book.

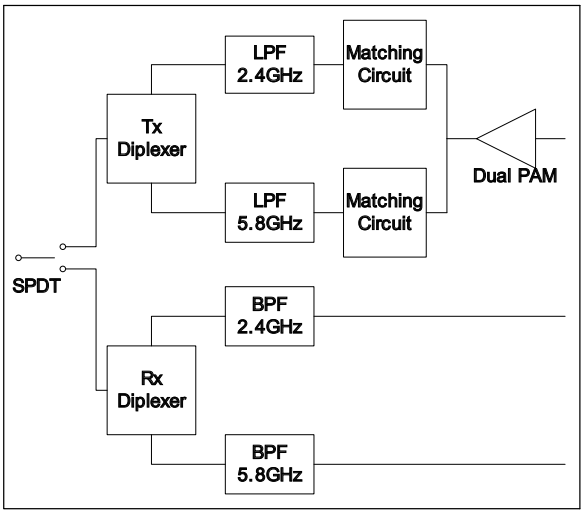

Fig. 1. Block diagram of W-LAN FEM.

2. Design for function blocks

2.1 Rx BPFs

The desired specifications of a LTCC BPF for low-band W-LAN FEM are as follows:
(a) A low insertion loss characteristic is required in the pass-band frequency range of 2.4 GHz – 2.5 GHz.
(b) A high attenuation is required in the stop-band frequencies of 1.91 GHz - 2.1 GHz, which can reduce the crosstalk from the image signal and local oscillator signal.
(c) A harmonic frequency in the range of 4.8 GHz – 5 GHz, needs to be reduced.
(d) The size of the BPF should be small, especially in it's thickness, to be successfully embedded in the miniaturized FEM.
The step impedance quarter-wavelength comb line type filter with two resonators was chosen to satisfy the required specifications mentioned above and to minimize its size. Each step impedance resonator is composed of a shunt capacitor and stripline. The shunt capacitor and the stripline are connected with a via of 100 um diameter. With this structure, the impedance of resonators can be seen as step impedance. Fig. 2 depicts the schematic and geometry of this 2nd order filter.
The input and output ports are directly connected to the resonator at the middle of the point connecting the stripline and the shunt capacitor. For the large amount of the magnetic coupling between those two resonators, two resonators are connected by a short line in the middle point of the strip line. Without this connecting line between two resonators, it is not large enough of the magnetic coupling because of the small thickness of this embedded BPF.
The design procedure of a high-band BPF is smilar to a low-band BPF. The pass-band and the rejection band of a high-band BPF range from 5.15 GHz to 5.85 GHz and from 2.4 GHz to 2.5 GHz, respectively. The size of a high-band BPF is smaller than a low-band BPF because wavelength is decreased with increased frequency and quater-wavelength in a BPF is depending on frequency.

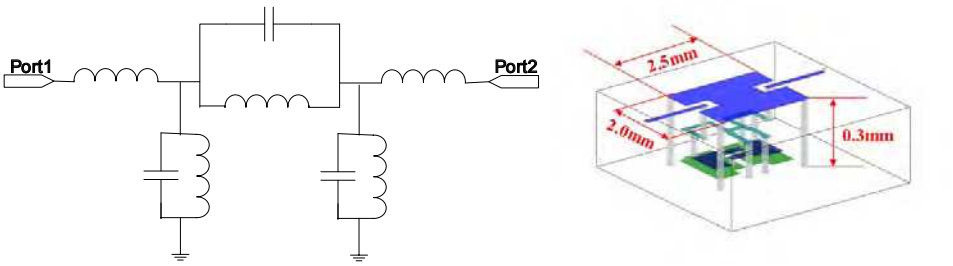

(a) (b)

Fig. 2. A BPF for : (a) schematic, (b) Geometry of the 2nd order band pass filter.

2.2 Rx Diplexer

The Rx diplexer is designed by using two fabricated BPFs. Each s-parameter extracted through measuring BPFs is adapted as depicted in fig. 3. The Rx diplexer can be divided into a low frequency path and a high frequency path. The low frequency path is composed of a series inductor, a shunt capacitor, and a BPF for low-band. High frequency path is composed of a series capacitor, a shunt inductor, and a BPF for high band as shown in fig. 3. A low-band path in a diplexer is similar to a schematic of a LPF and a high band path in a diplexer is similar to a schematic of high pass filter (HPF). The Rx diplexer employs conjugate impedance matching method in order to match low-band path and high-band path. Conjugate impedance matching is complementary approach between impedance of low-band and of high-band. This method is therefore sensitive to BPF's s-parameter or port impedance.

The Rx diplexer is designed as follows steps:

(a) 2.4 GHz ~ 2.5 GHz BPF is designed and fabricated.

(b) 5.15 GHz ~ 5.85 GHz BPF is designed and fabricated.

(c) S-parameters of two BPFs are extracted by measuring with probe station.

(d) Extracted S-parameters of two BPFs are substituted as basic blocks in order to design the Rx diplexer.

(e) The Rx diplexer is designed and optimized in level of schematic by employing S-parameters.

(f) The Rx diplexer is designed and optimized in level of 2.5-Dimensin (2.5-D) by employing S-parameters.

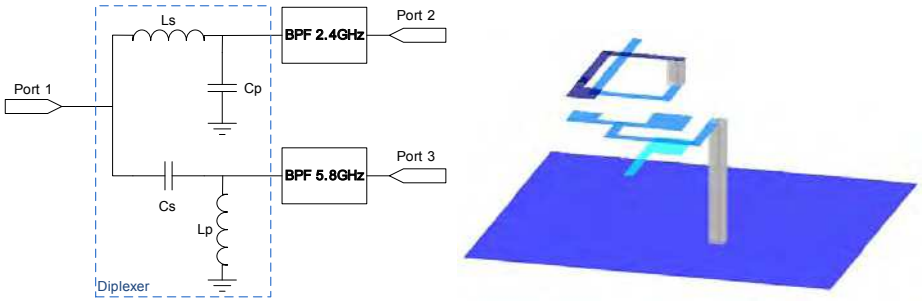

(a) (b)

Fig. 3. A Rx diplexer for : (a) schematic, (b) Geometry.

2.3 Tx matching stages

Most products for PAM IC are necessary that the output matching circuit are fabricated in outside of PCB. The input matching circuit is usually included in the PAM IC. This type is used in this book, so only output matching circuit is required. Fig. 4 shows a black diagram for output matching stage. The DC power is supplied from the output port through the inductor which plays a role to a RF choke, and RF signal goes through a 50 ohm transmission line, a shunt capacitor and a series capacitor which blocks the DC. The value of each component is too large and the length of transmission line is too long, so it is hard to make the LTCC module as small size. The equivalent circuit is proposed in this book and the input impedance of a matching circuit has to be extracted in order to find out optimal impedance. The input impedance of a matching circuit is measured and extracted by following two method : (a) by using a probe station, and (b) by using load pull equipment.

One method, by using a probe station, is explaned as following : At first, the matching circuit stage was designed and implemented on PCB. After finding the optimal matching circuit on PCB, the input impedance (S11) of matching circuit was measured by using the Ground-Signal-Ground (GSG) probe as shown in fig. 5 (a). The input impedance of a matching circuit may be extracted by Ground-Signal (GS) probe as depicted in fig. 5 (b). Table 1 is the measured result of the input impedance which was performed at the frequency 2.45 GHz depending on the variation of samples by using the GSG probes becuase each smaple has variation in input impedance.

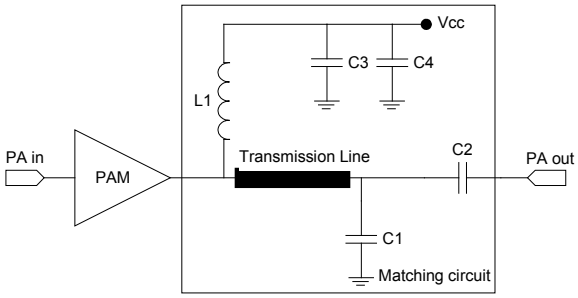

Fig. 4. Schematic of matching circuit.

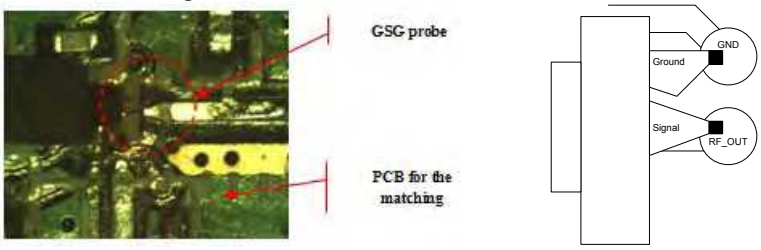

(a) (b)

Fig. 5. The example of measurement by using : (a) GSG, (b) GS.

	#1	#2	#3	#4	#5
Z	6.4 + j5.2	5.7 + j6.2	5.5 + j6.5	5.7 + j6.5	5.6 + j7.0

Table 1. Summary of input impedance for matching circuit on PCB

The average value from table 1 is 5.6 + j6.3. It is difficult to embed the inductor, capacitor, and transmission line in the LTCC. Therefore, the equivalent circuit as shown in fig. 6 is proposed. It consists of an inductor, a shunt capacitor, and a series capacitor. The equivalent value is induced to make the input impedance (S11) to be 5.6 + j6.3. The LTCC module was designed and implemented on basis of these.

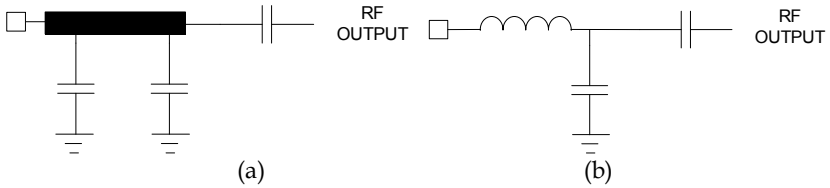

Fig. 6. The matching circuit for : (a) an orignal schematic. (b) a proposed schematic.

Second method, by using load pull equipment, is given as following : at first, load pull equimpment is set-up as depicted in fig. 7. Test set-up is composed of the input load pull equipment, the s-parameter box of compensation for physical transmission line as connection between a device under test (DUT) and output load pull equipment. At second, the PAM is mounted on PCB without the matching circuit. The impedance of matching circuit can be changed by controlling setting the load pull equipment. The maximum output power, the maximum gain, the power circle and the gain circle can be obtained by using load pull equipment. The measured maximum output power and gain are depicted in fig. 8. This result is obtained in condition of 22pF at DC bias line which effects the performance of a PAM. The input impedance of matching circuit is extracted by measuring several samples which are different from previous mentioned sample in previous paragraph. The average value of samples which is applied and the optimal impedance is 18.8 + j0.9. This value is the target of design and implementation

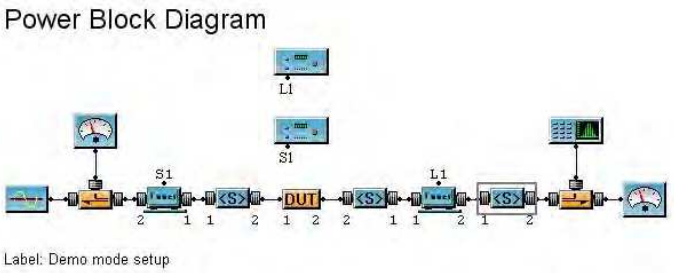

Fig. 7. Block diagram to extract the matching impedance by using load pull equipment

Fig. 9 shows the optimal gain circle and power circle depending on shunt capacitors in DC bias lines. The DC bias line of the PAM IC needs the shunt capacitor to reject DC bias noise. DC bias condition is major factor to meet the optimal performac of a PAM. The feedback in DC bias line causes the oscillation and cross modulation becaus of wanted signal and 2nd harmonic signal. Normally, shunt capacitors can remove the feedback signal. The value of the shunt capacitor is ranged from 100 pF to 1 nF. Fig. 9 depicts that the optimal impedance of matching circuit, maximum gain, and maximum power can be changed with variation of capacitor. In case of 100 pF, the maximum gain, the maximum power, and the optimal

impedance are 27.3 dB, 22.3 dBm, and 14.1 – j 37.0, respectively. Table 2 describes the summary data. In case of 22 pF, the maximum gain, the maximum power, and the optimal impedance are 27.7 dB, 22.7 dBm, and 17.7 – j 44.3, respectively. The optimal impedance, maximum gain, and maximum power are obtained when 22 pF as a shunt capcitor is connected with DC bias line.

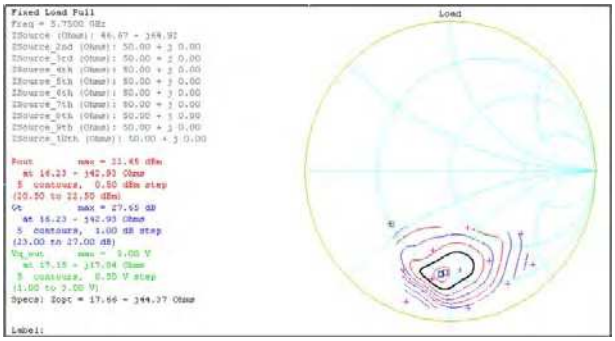

Fig. 8. Power and gain circle by using the load pull.

As a result, the optimal value can be obtained by trying to verify the various condition of DC bias line. These resuts mean that the power amplifier has different performance under DC bias condition. In order to merge the DC bias line, DC bias lines have to be maintain the isolation. The performance of a PAM is stable if isolation between ports are more than 20 dB. The optimal results can be extracted by attempting many trials at DC bias lines.

	100pF	22pF	5pF
Maximum Gain	27.28 dB	27.65 dB	24.99 dB
Maximum Pout	22.28 dBm	22.65 dBm	19.99 dBm
Optimal impedance	14.10 – j37.0	17.66 – j44.3	23.97 – j65.1

Table 2. Summary of Gain, Power, and Impedance depending on capacitors

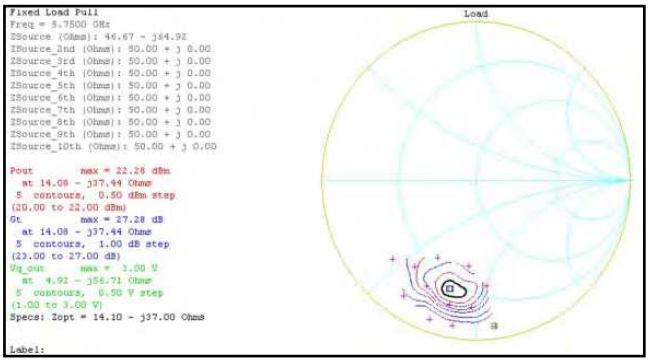

(a)

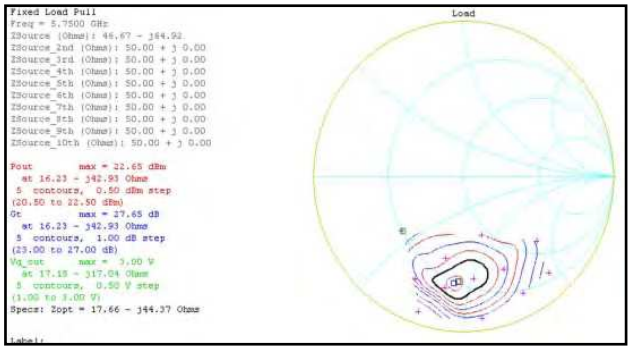

(b)

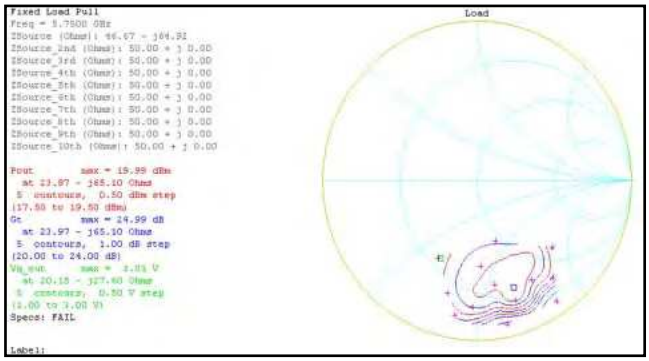

(c)

Fig. 9. Impedance of matching circuit depending shunt capacitors in DC bias line (a) 100 pF, (b) 22 pF, and (c) 5 pF.

Fig. 10 shows the presented a low-band matching equivalent circuit and a 3-D structure. This circuit is proposed and designed on basis of previous measured data. This circuit consists of a series inductor, series capacitor, and a shunt capacitor. L1 as a series inductor is given as 2 -turn coil shape in left side of fig. 9 (b). C1 as a shunt capacitor is induced by using parasitic capacitance. C2 as a series capacitor is given as parallel plate shape in center of fig. 9(b). 1-turn coil shape in right side of fig. 9 (b) is added to meet optimal impedance.

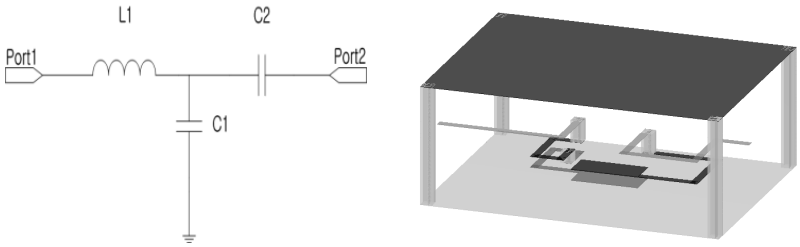

(a) (b)

Fig. 10. Low band matching circuit : (a) Equivalent circuit (b) 3-D geometry.

Fig. 11 illustrates the high-band matching circuit which is composed of transmission line. This methodology of circuit is different from low-band matching circuit. The matching circuit for low-band is designed and fabricated by employing lumped elements in LTCC, but the matching circuit for high-band suffers from being designed by using lumped element because of parasitic capacitance at high frequency. As mentioned in previous, the matching impedance for high-band is designed by same procedure for low-band matching circuit. The optimal impedance of the output matching is given as 18.1 + j 5.9 at high-band. This target can be implemented by using an ideal shunt capacitor with 0.5 pF, but this can't be designed in the LTCC substrate. Because the parasitic shunt capacitor is more than 0.8 pF in W-LAN high frequency. This book proposed this matching circuit with the geometry of transmission line. The impedance and electrical length of the designed transmission line are 27.05 ohm and 82.8 degree, respectively. Fig. 11 (b) depicts 3-D geometry of strip line.

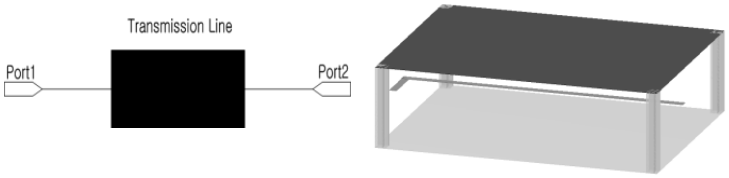

(a) (b)

Fig. 11. High band matching circuit: (a) Equivalent circuit (b) 3-D geometry.

2.4 Tx LPFs

The permittivity and dielectric loss tangent of LTCC substrate are 9.0 and 0.0035, respectively. These LPFs play a role to reject 2nd harmonic of fundamental wireless LAN signal. In case of a low-band LPF, the pass band of a low-band LPF ranges from 2.4 GHz and 2.5 GHz. The stop band of low-band LPF ranges from 4.8 GHz and 5 GHz. In case of a high-band LPF, the pass band of a high-band LPF is given from 5.15 GHz to 5.85 GHz and the stop band of a LPF ranges from 10.3 GHz and 11.7 GHz.

A low-band LPF composed of inductors and capacitors as shape as T-junction or ladder. The size of each component according to this schematic is large, so it is difficult to make small module and to fabricate a LPF. The equivalent circuit for a low-band LPF as depicted in fig. 12 (a) is proposed. The equivalent circuit has two transmission zeros on basis of 3rd LPF as shown in fig. 12 (a). Transmission zero is generated by a series capacitor and a series inductor. Fig. 12 (b) illustrates a 3-D geometry for a low-band LPF. A shunt capacitor is designed by using one plate and a ground plane as depict in low side of fig. 12 (b).

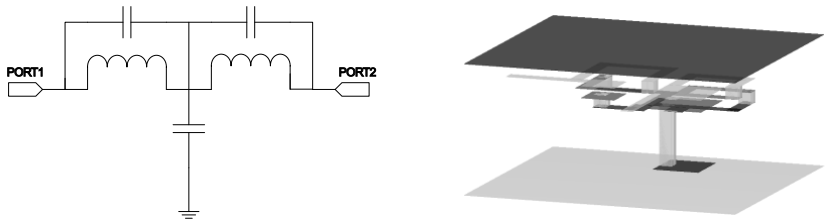

(a) (b)

Fig. 12. Proposed low-band LPF : (a) schematic, (b) 3-D geometry.

A high-band LPF consists of inductors and capacitors. As mentioned in low-band LPF, an equivalent circuit of a high-band LPF is proposed as depicted in fig. 13. The proposed circuit adds two shunt capacitors in comparison to the low-band LPF in order to improve the characteristic of rejection. A high-band LPF is sensitive to dimension of designed components because the many parasitic facts occur in high frequency. For example, a series capacitor is composed of two parallel plates which occurs parasitic capacitance from ground plane to parallel plates in high frequency. The design and the control of parasitic component are key fact. RF components in high frequency are designed to avoid these facts, but these parasitic capacitors are employed in this book instead of avoiding it. A proposed high-band LPF is composed of series inductors, series capacitors, and shunt capacitors which are parasitic capacitors. Shunt capacitors as depicted in fig. 13 (a) don't appear in 3-D geometry as depicted in fig. 13 (b).

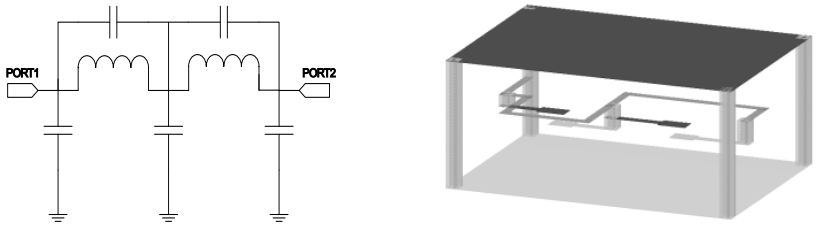

(a) (b)

Fig. 13. Proposed high-band LPF : (a) schematic, (b) 3-D geometry.

2.5 Tx Diplexer

The concept of Tx diplexer and the flowchart for Tx part is similar to Rx part as mentioned in 2.2. The results of Tx LPFs are only employed instead of Rx BPFs. The Tx diplexer is designed as following step:

(a) 2.4 GHz ~ 2.5 GHz LPF is designed and fabricated.

(b) 5.15 GHz ~ 5.85 GHz LPF is designed and fabricated.

(c) S-parameters of two LPFs are extracted by measuring with probe station.

(d) Extracted S-parameters of two LPFs are substituted as basic blocks in order to design the Tx diplexer.

(e) The Tx diplexer is designed and optimized in level of schematic by employing S-parameters,

(f) The Tx diplexer is designed and optimized in level of 2.5-Dimensinal (2.5-D) by employing S-parameters.

The Tx diplexer has the schematic and geometry as depicted in fig. 14. Each s-parameter box in fig. 14 (a) is obtained from measured Tx LPFs. The low frequency path is composed of a series inductor, and a Tx LPF for low-band. High frequency path is composed of two series capacitor, a shunt inductor, and a LPF for high-band. The part of low path consists of a series inductor and shunt capacitor but shunt capacitor is removed because a low-band LPF doesn't have 50 ohm but including shunt capacitance. Ls1 and Lp1 are designed by lines and series capacitors have shape of two parallel plates as illustrated in fig. 14 (b).

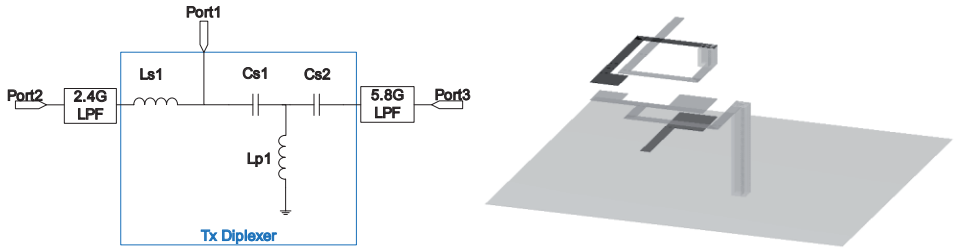

(a) (b)

Fig. 14. Design for a Tx diplexer (a) equivalent circuit (b) 3-D layers.

3. Module design and fabrication

The whole module is composed of a SPDT IC, a PAM IC, and a LTCC substrate which integrates a Rx diplexer, a Tx diplexer, two Rx BPFs, two Tx LPFs, and two matching circuits. LTCC green sheets (X200) are obtained from Heraus company. Its dielectric constant and loss tangent are given as 9 and 0.005, respectively. The size of LTCC substrate and whole module are given as 7.0 mm × 6.0 mm × 0.7 mm and 7.0 mm × 6.0 mm × 1.2 mm, respectively. The thickness of ICs is approximately 0.5 mm. Fig. 15 (a) illustrates the overall structure of the proposed module and the PAM, the SPDT, and external components are mounted on top layer. The PAM (μPG2317T5J) and SPDT (μPG2163T5N) are supplied from NEC company. GND planes are placed in the second layer, bottom, and middle. It distinguishes each component and isolates each part in order to maintain the performance of the components. Fig. 15 (b) shows the photograph of the implemented module.

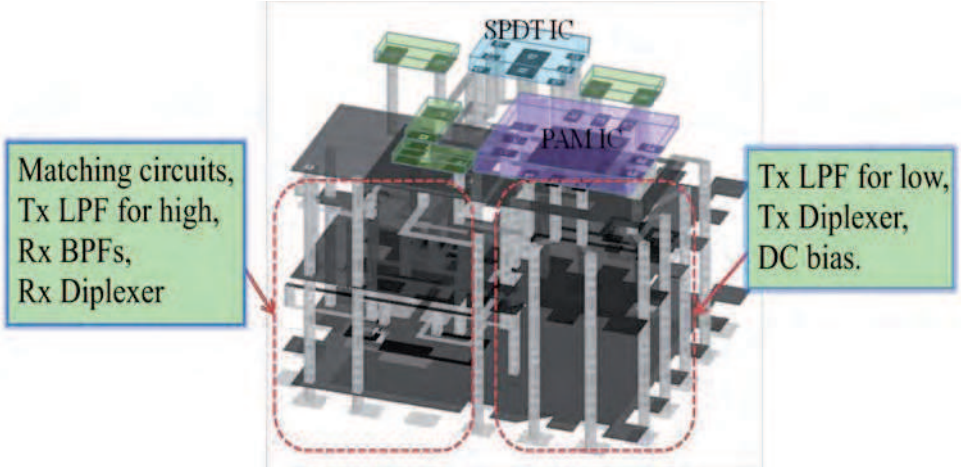

(a)

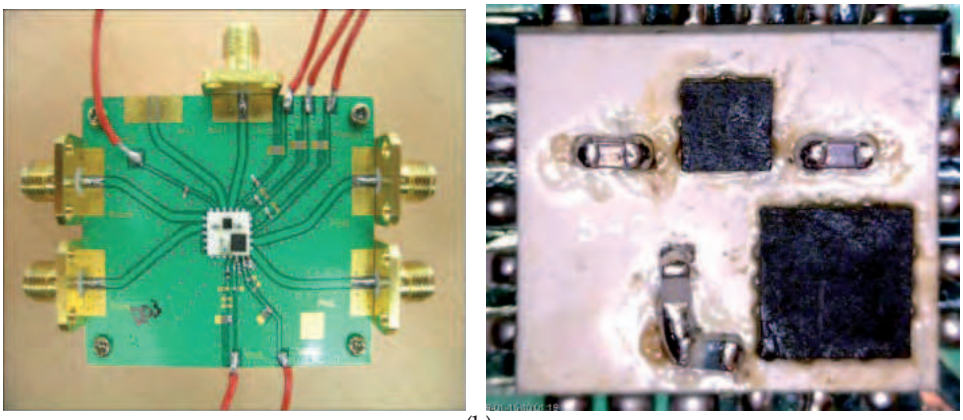

(b)

Fig. 15. W-LAN FEM: (a) 3-D geometry (b) Photograph

4. Measured performance

The implemented 802.11 a/b/g FEM with a PAM was measured by Agilent's N5230 network analyzer, Agilent's E4432B signal generator, and Agilent's E4407B spectrum analyzer.

Two Rx BPFs, two Tx LPFs, and two matching stage are individually fabricated and measured because measured results of those can't be obtained in the full module. Fig. 16 displays the simulated and measured data for a low-band BPF and a high-band BPF. Blue trace, black trace, solid trace, and dash trace are given as insertion loss, return loss, a simulated line, and a measured line as illustrated in fig. 16. A low-band BPF shows simulation and measurement has little difference. Insertion loss, rejection at 1.9 GHz, and rejection at IEEE 802.11 a are better than 1.3 dB, 25 dB and 20 dB, respectively.

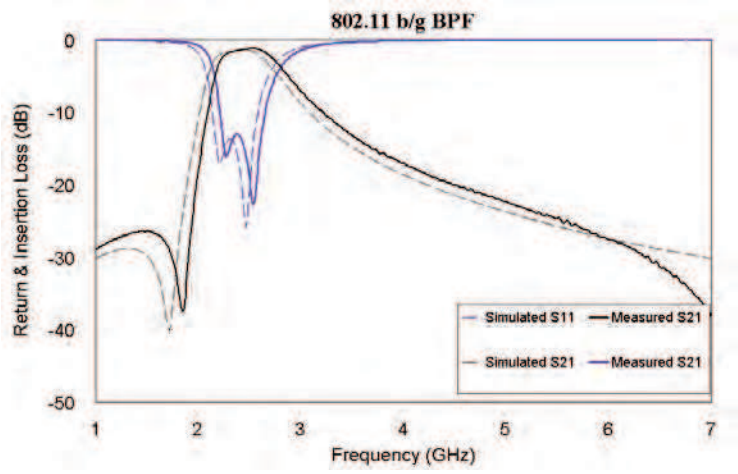

(a)

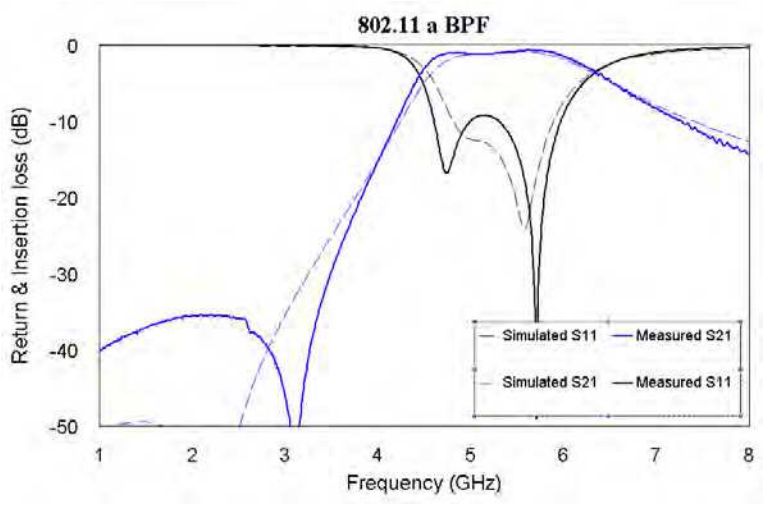

(b)

Fig. 16. Simulated and measured data for : (a) a low-band LPF, (b) a high-band LPF.

Fig. 17 illustrates the simulated and measured data for two Tx LFPs. Blue line, black line, solid line, and dash line are given as insertion loss, return loss, a simulated line, and a measured line as illustrated in fig. 17, respectively. Insertion loss and 2nd harmonic rejection for low- band LPF are 0.43 dB and 32 dB. In case of high band, the insertion loss and 2nd harmonic rejection are 0.64 dB and 32.6 dB, respectively.

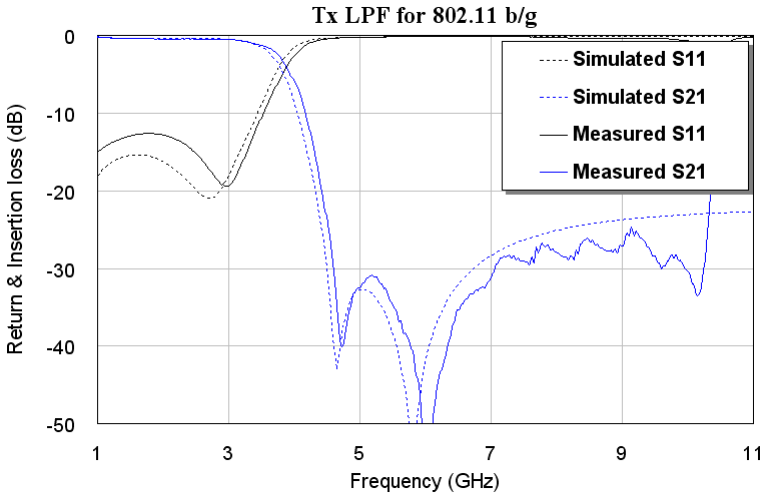

(a)

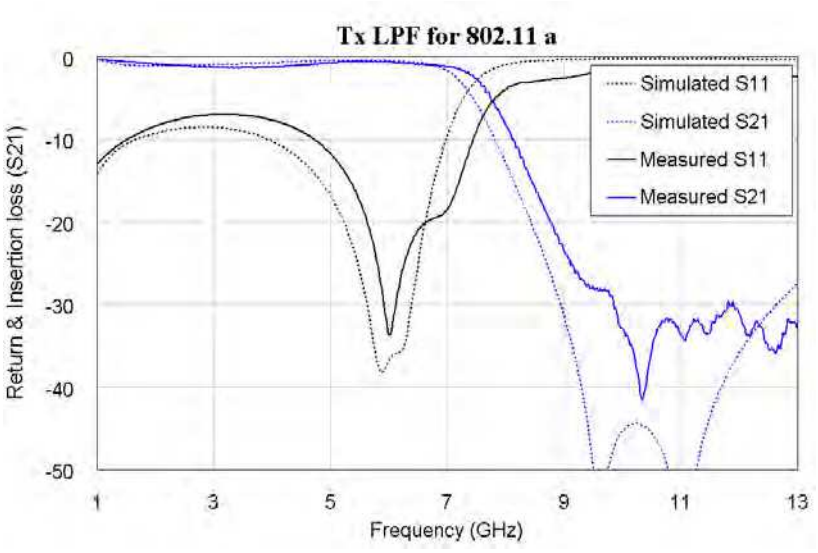

(b)

Fig. 17. Simulated and Measured data from LPF: (a) 802.11 b/g (b) 802.11 a

The simulated and measured data for two matching circuit are shown in fig. 18. Red trace and blue trace means simulation and measurement, respectively. Input impedance of matching circuit between required frequency ranges is measured and the results meet the target impedance.

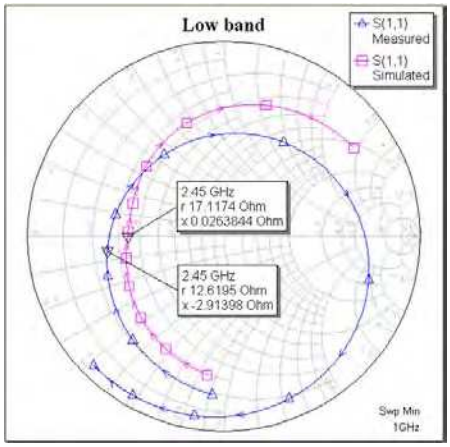

(a)

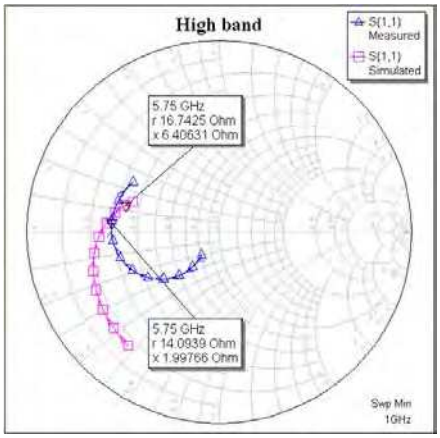

(b)

Fig. 18. Simulated and measured data from matching circuit.

Fig. 19 (a) illustrate measured data from Rx part which includes the SPDT switch, Rx diplexer, and two BPFs. Dash line and solid line display simulated and measured data, respectively. Black line, blue line, and green line express return loss, insertion loss of low-band, respectively. Insertion loss is less than 3.3 dB and return loss is better than 15.5 dB in each pass band as described in table 3. Fig. 19 (b) show measured data from Tx part which includes the SPDT switch, the Tx diplexer and two LPFs. Insertion loss is less than 2.6 dB and return loss is better than 11.3 dB as summarized in table 4.

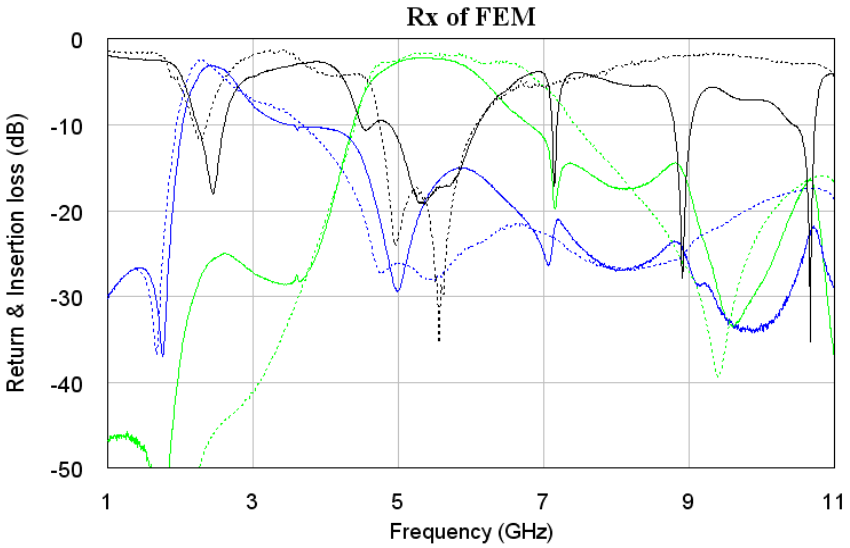

(a)

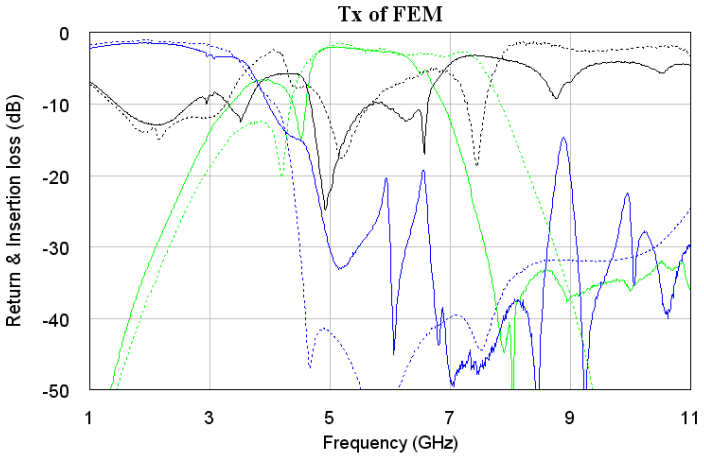

(b)

Fig. 19. Simulated and Measured data: (a) Rx part (b) Tx part.

Rx part	(Rx Diplexer + 2G BPF + 5G BPF+ SPDT)	
	2.4 GHz ~ 2.5 GHz	5.15 GHz ~ 5.85 GHz
Return loss	16.5 ~15.5 dB	16.5 ~15.5 dB
Insertion loss	3.11 ~3.26 dB	2.32 ~2.73 dB
Rejection	17.03 dB @ 5.50GHz 18.67 dB @ 1.90GHz	25.64 dB @ 2.45GHz 44.12 dB @ 1.90GHz

Table 3. Summary of measurement for Rx Part

Tx Part	Tx Diplexer + 2G LPF + 5G LPF + SPDT	
	2.4 GHz ~ 2.5 GHz	5.15 GHz ~ 5.85 GHz
Return loss	12.07 ~11.34 dB	16.98 ~9.93 dB
Insertion loss	1.72 ~1.84 dB	2.07 ~2.57 dB
Rejection	30.46 dB @ 5GHz	35.09 dB @ 11GHz

Table 4. Summary of measurement for Tx Part

(a)

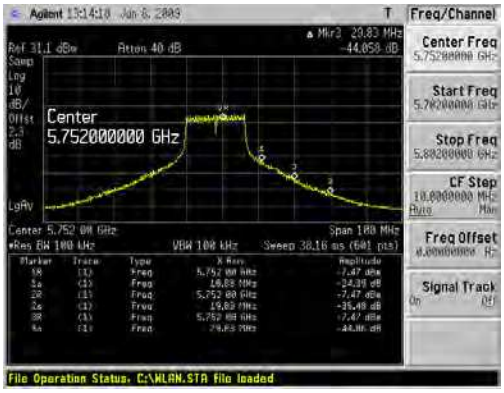

(b)

Fig. 20. RF output spectrum (@18dBm) for: (a) 802.11 b/g (b) 802.11 a

The Tx performance of implemented module was measured at the 18 dBm output power. In case of low-band, measured adjacent-channel power ratios (ACPRs) of the presented module at first side-lobe and second side-lobe are -30.2 dBc and -50.0 dBc with 23.1 dB gain as shown in fig. 20 (a). In case of high band, first side-lobe, second side-lobe and third side-lobe are -24.3 dBc, -35.4 dBc, and -44.8 dBc with 24.5 dB gain as shown in fig. 20 (b), respectively.

5. Conclusion

The 802.11 a/b/g FEM with PAM was designed and implemented. It was composed of a SPDT switch, a Rx diplexer, two Rx BPFs, a Tx diplexer, two Tx LPFs, two matching circuits, and a dual-band PAM. The performance of the module was satisfied with IEEE 802.11 a/b/g regulation and the size of the module is very compact.

6. References

Dongsu Kim, D.H Kim, J.I. Ryu, and J.C Kim, "Highly integrated triplexers for WiMAX applications," *2008 MTT-S*, pp. 614-617, 2008.

J. I. Ryu, D. Kim, H. M. Cho, and J. C . Kim, "Implementation of WLAN front end module with a power amplifier," *in Proceeding of the Asia Pacific Microwave Conf.*, pp. 99-102, vol.1,2007..

D. H. Kim, D. Kim, J. I. Ryu, J. C. Kim, C. D. Park, I. S. Song, "Implementation of an LTCC Quad-band module for WLAN and WiMAX applications," *Eur. Microwave. Conf.*, PP.614-617, 2008.

J. I. Ryu, D. Kim, and J. C . Kim, "Isolation Effect Between DC supply Voltage Signal Lines in Wireless LAN Module," *in Proceeding of the 20th Inter. Zurich Sym.*, pp. 385-388, 2009.

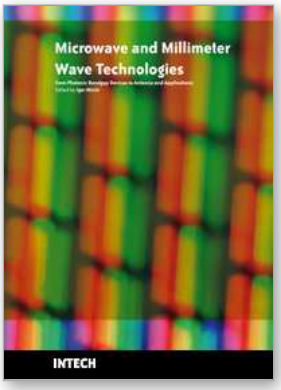

Microwave and Millimeter Wave Technologies from Photonic Bandgap Devices to Antenna and Applications

Edited by Igor Minin

ISBN 978-953-7619-66-4
Hard cover, 468 pages
Publisher InTech
Published online 01, March, 2010
Published in print edition March, 2010

The book deals with modern developments in microwave and millimeter wave technologies, presenting a wide selection of different topics within this interesting area. From a description of the evolution of technological processes for the design of passive functions in milimetre-wave frequency range, to different applications and different materials evaluation, the book offers an extensive view of the current trends in the field. Hopefully the book will attract more interest in microwave and millimeter wave technologies and simulate new ideas on this fascinating subject.

How to reference

In order to correctly reference this scholarly work, feel free to copy and paste the following:

Jong-In Ryu, Dongsu Kim and Jun-Chul Kim (2010). Implementation of the Front-End-Module with a Power Amplifier for Wireless LAN, Microwave and Millimeter Wave Technologies from Photonic Bandgap Devices to Antenna and Applications, Igor Minin (Ed.), ISBN: 978-953-7619-66-4, InTech, Available from: http://www.intechopen.com/books/microwave-and-millimeter-wave-technologies-from-photonic-bandgap-devices-to-antenna-and-applications/implementation-of-the-front-end-module-with-a-power-amplifier-for-wireless-lan

INTECH
open science | open minds

InTech Europe
University Campus STeP Ri
Slavka Krautzeka 83/A
51000 Rijeka, Croatia
Phone: +385 (51) 770 447
Fax: +385 (51) 686 166
www.intechopen.com

InTech China
Unit 405, Office Block, Hotel Equatorial Shanghai
No.65, Yan An Road (West), Shanghai, 200040, China
中国上海市延安西路65号上海国际贵都大饭店办公楼405单元
Phone: +86-21-62489820
Fax: +86-21-62489821